16th Mediterranean Conference on Control and Automation
Congress Centre, Ajaccio, France
June 25-27, 2008

Modeling and Control of a Triangular Floating Platform Driven by Rotating Jets

Filoktimon Repoulias, Kostas Vlachos, and Evangelos Papadopoulos, *Senior Member, IEEE*

***Abstract*—In this paper, we consider the dynamic modeling and the practical implementation of an autonomous dynamic positioning scheme, i.e., the stabilization of linear and angular velocities as well as the position and orientation, of a floating sea triangular platform. The required, closed-loop force and moment must be provided by three rotating pump jets, located at the bottom of three partly submerged cylinders at the corners of the platform. With this control configuration the platform is overactuated, i.e., it has more control inputs than degrees of freedom (DOF). We present the initial design of a control allocation scheme that allows goal realization without violating thruster capabilities. Simulation results are presented that demonstrate the performance of the controller, and the allocation scheme employed.**

***Index Terms*— Floating platform control, rotating jets driven platform, control allocation.**

I. Introduction

FLOATING platforms are widely used in offshore petroleum industry, as portable pipeline systems, as research, in-the-field laboratories, etc, [1]. These platforms must be kept stationary at a desired position and orientation in order to accomplish their task. Therefore, these platforms are equipped with appropriate actuation systems that provide the necessary dynamic positioning to counterbalance the sea waves and currents, and the uncertainties in modeling the dynamics of the platform. Floating platform dynamics are inherently nonlinear due to the rigid body dynamics and, more importantly, due to the strong hydrodynamic interactions, [2]. Hence, in order to design efficient closed-loop controllers, nonlinear techniques must be adopted. Control allocation schemes must also be designed; usually, such vessels have redundant actuators, i.e., they have more control inputs than DOF yielding an overactuated control system. Thus, the closed-loop control forces and moments need to be efficiently distributed to the actuators in such a way that the control objective is realized without violating the thrusters' capability. The above problem leads, in general, to a constrained optimization problem that is hard to solve using even state-of-the-art iterative numerical optimization software in a safety-critical real-time system with limiting processing capacity, [3]. Though, real-time iterative optimization solutions have been proposed [4], [5], and [6]. Optimal thrust allocation has been addressed in [7]. Thrusters that can be rotated, and thus produce two force components in the horizontal plane, are usually mounted under the hull of the vessel. Optimization schemes for such actuation configurations have been proposed for example in [8]. In [9], controllability problems regarding the plane motion are studied.

In this paper, we consider the dynamic modeling and the stabilization of linear and angular velocities as well as the position and orientation, of a floating triangular platform moving on the sea surface, see Fig. 1. Our main goal is the practical implementation of such an autonomous dynamic positioning scheme. The required, closed-loop force and moment is provided by three rotating pump jets, located at the bottom of three partly submerged cylinders at the corners of the platform. The system is overactuated, i.e., it has more control inputs than degrees of freedom (DOF). Hence, we design a properly control allocation scheme in order for the control objective to be realized without violating the thrusters capability. This scheme is based on the maximization of the determinant of the transformation matrix relating the control forces and the jet thrust, which is a novel approach. This methodology provides a fast, reliable, and computationally inexpensive algorithm related to the complex, on-line, iterative ones. Simulation results are finally presented to demonstrate the performance of the controller, and allocation scheme.

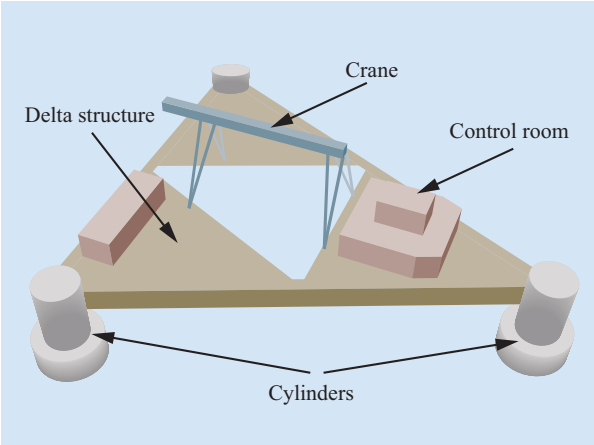

Figure 1. A 3D representation of the triangular platform.

Manuscript received February 03, 2008. This work was supported by the VERENIKI program with funding from the Hellenic Ministry of Education and Religion and the European Union.

F. Repoulias, K. Vlachos, and E. Papadopoulos are with the Department of Mechanical Engineering, National Technical University of Athens, 15780 Athens, Greece, (e-mail: {firepoul; kostaswl; egpapado}@central.ntua.gr).

II. Platform System Description

In this section, a general description of the floating platform is given, along with its geometry, its kinematics, and its dynamics.

A. General Description

A 3D representation of the platform is shown in Fig. 1. It consists of a triangular structure mounted on three double-cylinders, one at each corner of the structure. The plane of the triangle is parallel to the sea surface. These cylinders provide the necessary buoyancy since part of their body is immersed. The actuation of the platform is realized utilizing pump jets at the bottom of the three cylinders, fully submerged. A diesel engine drives each pump, while an electro-hydraulic motor can rotate the jet providing vectored thrust. Currently, the platform is under construction. It will be used during the assembly of the deep sea high-energy neutrino telescope "NESTOR", [10].

B. Geometry

The main body of the structure has the shape of an isosceles triangle with $L_{AB} = L_{AC}$ and L_{BC} the length of the base, Fig. 2.

The structure has its center of mass (CM) coinciding with point G, along the symmetry axis at a distance d_{AG} from the vertex A.

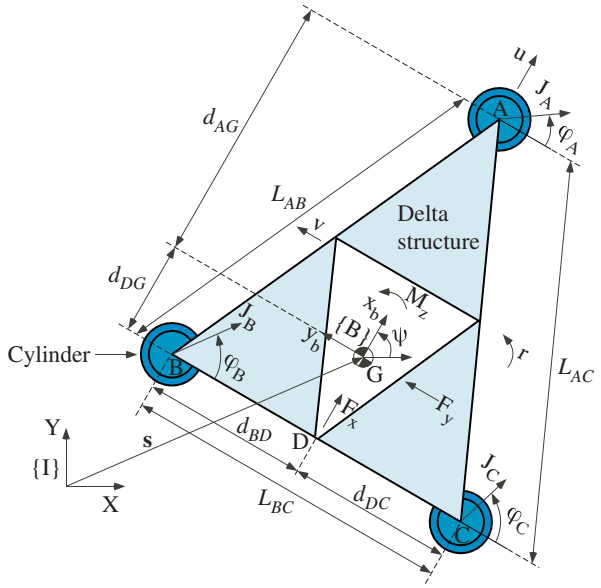

Figure 2. A 2D representation of the platform.

Further geometric characteristics are: the distances between the vertices B, C and the mid point D of the segment BC, i.e., $d_{BD} = d_{DC}$; the distance d_{DG} between the points D and G; the height H_{uc} and the radius R_{uc} of the upper cylinder which is partly submerged with h the variable height above the sea surface; and the height H_{lc} and the radius R_{lc} of the lower cylinder which is fully submerged, Fig. 3.

C. Kinematics

To describe the kinematics of plane motion, two reference frames are employed, the inertial reference frame $\{I\}$ and the body-fixed frame $\{B\}$, see Fig. 2. As shown, the origin of $\{B\}$ frame coincides with the platform CM. The x_b body axis is aligned with the symmetry axis of the platform, the y_b points left, and z_b points upwards. Hence, the kinematics equations of the plane motion are:

$$\dot{\mathbf{x}} = \mathbf{R}\mathbf{v} \tag{1a}$$

where

$$\dot{\mathbf{x}} = [\dot{x}, \dot{y}, \dot{\psi}]^T \tag{1b}$$

$$\mathbf{v} = [u, \upsilon, r]^T \tag{1c}$$

$$\mathbf{R} = \begin{bmatrix} c\psi & -s\psi & 0 \\ s\psi & c\psi & 0 \\ 0 & 0 & 1 \end{bmatrix} \tag{1d}$$

with $s\cdot = \sin(\cdot)$, $c\cdot = \cos(\cdot)$. In (1), x and y represent the inertial coordinates of the CM and ψ the orientation of $\{B\}$ with respect to the $\{I\}$ frame; u and υ are the surge and sway velocities respectively, defined in the body-fixed frame, and r is the yaw (angular) velocity of the platform, Fig. 2.

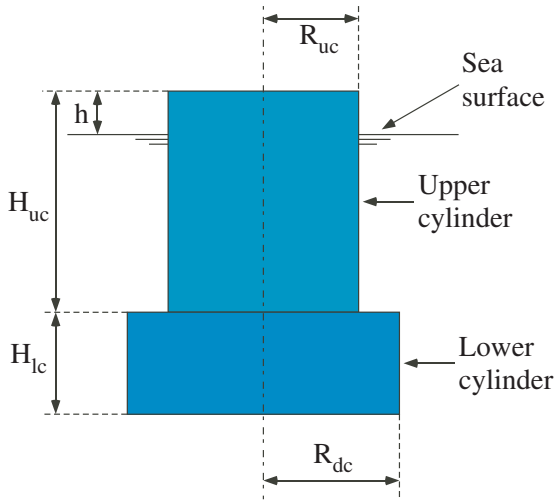

Figure 3. A side view of the double-cylinder structure.

Due to the fact that the hydrodynamics interactions are between the water and the submerged part of the cylinders, we also need the kinematics relations between the cylinders and the CM in order to derive equations for the hydrodynamic forces and moments. First, we introduce some necessary notations: ${}^B\mathbf{s}_{A/G}$ is the position of point A with respect to G expressed in frame $\{B\}$, and ${}^B\mathbf{s}_{B/G}$, and ${}^B\mathbf{s}_{C/G}$ have similar meaning; ${}^B\mathbf{v}_G = [u, \upsilon]^T$ is the linear

velocity vector of the CM, ${}^B\mathbf{a}_G = {}^B\dot{\mathbf{v}}_G$ is the linear acceleration vector, and $\alpha = \dot{r}$ is the angular acceleration, all expressed in frame $\{B\}$. Then, the following geometric relations hold:

$${}^B\mathbf{s}_{A/G} = [d_{AG}, 0]^T \tag{2a}$$

$${}^B\mathbf{s}_{B/G} = [-d_{DG}, d_{BD}]^T \tag{2b}$$

$${}^B\mathbf{s}_{C/G} = [-d_{DG}, -d_{DC}]^T \tag{2c}$$

Velocities and accelerations are given by:

$${}^B\mathbf{v}_A = [u, \upsilon + rd_{AG}]^T \tag{3a}$$

$${}^B\mathbf{a}_A = [\dot{u} - r^2 d_{AG}, \dot{\upsilon} + \alpha d_{AG}]^T \tag{3b}$$

$${}^B\mathbf{v}_B = [u - rd_{BD}, \upsilon - rd_{DG}]^T \tag{3c}$$

$${}^B\mathbf{a}_B = [\dot{u} - \alpha d_{BD} + r^2 d_{DG}, \dot{\upsilon} - \alpha d_{DG} - r^2 d_{BD}]^T \tag{3d}$$

$${}^B\mathbf{v}_C = [u + rd_{DC}, \upsilon - rd_{DG}]^T \tag{3f}$$

$${}^B\mathbf{a}_C = [\dot{u} + \alpha d_{DC} + r^2 d_{DG}, \dot{\upsilon} - \alpha d_{DG} + r^2 d_{DC}]^T \tag{3g}$$

D. Dynamics

The structure is statically balanced in the vertical direction because the weight equals buoyancy: specifically, when the weight of the structure increases –within certain bounds– the cylinders are submerged further, yielding increased buoyancy and vice-versa, see Fig. 3. From this static balance, the height above the surface is computed as:

$$h = H_{uc} - (1/R_{uc}^2)(m/(3\pi\rho) - R_{lc}^2 H_{lc}) \tag{4}$$

where ρ is the water density and m is the mass of the structure. The hydrodynamic forces are due to the motion of the cylinders into the water: the added mass force is a linear function of the acceleration of the cylinder, while the drag force is a quadratic function of the cylinder velocity. These forces are modeled according to Morison's Equation [11]. As an example, we derive here the force on a cylinder at point A, expressed in body-fixed frame $\{B\}$:

$$\begin{aligned}\mathbf{f}_A = &-C_A \pi\rho[R_{uc}^2(H_{uc} - h) + R_{lc}^2 H_{lc}]\,{}^B\mathbf{a}_A \\ &- C_D\rho[R_{uc}(H_{uc} - h) + R_{lc}H_{lc}]\left\|{}^B\mathbf{v}_A\right\|{}^B\mathbf{v}_A\end{aligned} \tag{5}$$

where C_A is the added mass coefficient and C_D the drag coefficient. The forces on the cylinder are equivalent with an equal force and a moment acting on the CM. For example, the force in (5) gives

$$\mathrm{t}_G = {}^B\mathbf{s}_{A/G} \times \mathbf{f}_A \tag{6}$$

It is already mentioned that the jets can provide vectored thrust and thus more flexibility in control design, Fig. 2. The magnitudes of the thrusts are denoted by J_A, J_B, and J_C while φ_A, φ_B, and φ_C denote the corresponding rotation variables. These thrusts provide control forces in x_b and y_b axes, F_x and F_y respectively acting on the CM, and torque M_z about z_b, according to the linear transformation:

$$\mathrm{t}_c = \mathbf{B}(\varphi_A, \varphi_B, \varphi_C)\mathbf{J} \tag{7a}$$

where

$$\mathrm{t}_c = [F_x, F_y, M_z]^T \tag{7b}$$

$$\mathbf{B} = \begin{bmatrix} s\varphi_A & s\varphi_B & s\varphi_C \\ -c\varphi_A & -c\varphi_B & -c\varphi_C \\ -d_{AG}c\varphi_A & d_{DG}c\varphi_B - d_{DC}s\varphi_B & d_{DG}c\varphi_C + d_{DC}s\varphi_C \end{bmatrix} \tag{7c}$$

$$\mathbf{J} = [J_A, J_B, J_C]^T \tag{7d}$$

Using the above computations we derive the equations of motion of the platform in plane motion, expressed in body-fixed frame $\{B\}$:

$$\mathbf{M}\dot{\mathbf{v}} = \mathbf{f} + \mathrm{t}_c \tag{8a}$$

where, the mass and added mass matrix is

$$\mathbf{M} = \begin{bmatrix} m - 3m_A & 0 & 0 \\ 0 & m - 3m_A & (2d_{DG} - d_{AG})m_A \\ 0 & (2d_{DG} - d_{AG})m_A & I_{zz} - (d_{AG}^2 + 2d_{BD}^2 + 2d_{DG}^2)m_A \end{bmatrix} \tag{8b}$$

with m_A is the coefficient of the acceleration in (5), and I_{zz} the mass moment of inertia about the z_b axis. Also,

$$\dot{\mathbf{v}} = [\dot{u}, \dot{\upsilon}, \dot{r}]^T \tag{8c}$$

$$\mathbf{f} = [f_x, f_y, f_z]^T \tag{8d}$$

where $\mathbf{f}$ is a nonlinear function of the velocities of the system not written here due to space limitations.

III. Closed Loop Control Design

In this section, we design a closed loop controller for dynamic positioning purposes. We assume as closed control input the vector t_c. In the next section we transform this in jet $\mathbf{J}$ vector requirements. From (8a) it is

$$\dot{\mathbf{v}} = \mathbf{M}^{-1}(\mathbf{f} + \mathrm{t}_c) \tag{9}$$

yielding three scalar equations

$$\dot{u} = f_{u1} + f_{u2}F_x \tag{10a}$$

$$\dot{\upsilon} = f_{\upsilon 1} + f_{\upsilon 2}M_z + f_{\upsilon 3}F_y \tag{10b}$$

$$\dot{r} = f_{r1} + f_{r2}F_y + f_{r3}M_z \tag{10c}$$

where the various f's are functions of the states. We observe that there are input couplings in (10b) and (10c) but the corresponding coefficients $f_{\upsilon 2}$ and f_{r2} are very small,

justifying the consideration of $f_{v2}M_z$ and $f_{r2}F_y$ as small disturbances that are bounded and that can be counteracted by a robust closed loop controller. Hence, in the last two equations the control design variables are F_y and M_z respectively. Setting

$$F_x = 1/f_{u2}(\alpha - f_{u1}f_{u2}) \tag{11a}$$

$$F_y = 1/f_{v3}(\beta - f_{v1}f_{v3}) \tag{11b}$$

$$M_z = 1/f_{r3}(\gamma - f_{r1}f_{r3}) \tag{11c}$$

with α, β, and γ auxiliary control design variables, we have the system

$$\dot{u} = \alpha \tag{12a}$$

$$\dot{v} = \beta + f_{v2}M_z \tag{12b}$$

$$\dot{r} = \gamma + f_{r2}F_y \tag{12c}$$

From (1a) we can write

$$\ddot{\mathbf{x}} = \dot{\mathbf{R}}\mathbf{v} + \mathbf{R}\dot{\mathbf{v}} \tag{13}$$

Setting the control variables α, β, and γ from (12) as

$$\dot{\mathbf{v}} = \mathbf{R}^T(\mathbf{f}_{fb} - \dot{\mathbf{R}}\mathbf{v}) \tag{14}$$

selecting the feedback such as to include integral action, i.e.

$$\begin{aligned}\mathbf{f}_{fb} = {} & [\ddot{x}_R, \ddot{y}_R, \ddot{\psi}_R]^T - \mathbf{K}_D[\dot{x}-\dot{x}_R, \dot{y}_R-\dot{y}_R, \dot{\psi}-\dot{\psi}_R]^T \\ & -\mathbf{K}_P[x-x_R, y_R-y_R, \psi-\psi_R]^T \\ & -\mathbf{K}_I\int_0^t [x-x_R, y_R-y_R, \psi-\psi_R]^T dt\end{aligned} \tag{15}$$

with the following positive definite diagonal gain matrices $\mathbf{K}_D = diag\{k_{dx}, k_{dy}, k_{d\psi}\}$, $\mathbf{K}_P = diag\{k_{px}, k_{py}, k_{p\psi}\}$, $\mathbf{K}_I = diag\{k_{ix}, k_{iy}, k_{i\psi}\}$, then the controlled system becomes,

$$\begin{aligned}\ddot{x} - \ddot{x}_R = {} & -k_{dx}(\dot{x}-\dot{x}_R) - k_{px}(x-x_R) \\ & -k_{ix}\int_0^t (x-x_R)dt + \varepsilon_x\end{aligned} \tag{16a}$$

$$\begin{aligned}\ddot{y} - \ddot{y}_R = {} & -k_{dy}(\dot{y}-\dot{y}_R) - k_{py}(y-y_R) \\ & -k_{iy}\int_0^t (y-y_R)dt + \varepsilon_y\end{aligned} \tag{16b}$$

$$\begin{aligned}\ddot{\psi} - \ddot{\psi}_R = {} & -k_{d\psi}(\dot{\psi}-\dot{\psi}_R) - k_{p\psi}(\psi-\psi_R) \\ & -k_{i\psi}\int_0^t (\psi-\psi_R)dt + \varepsilon_\psi\end{aligned} \tag{16c}$$

In (16), "R" denotes a reference (desired) variable, and ε_x, ε_y, and ε_ψ are small and bounded disturbances.

IV. Control Allocation

In this section, the proposed control allocation scheme that has been implemented is illustrated. The goal is to distribute the closed-loop control forces and moments efficiently to the actuators in such a way that the control objective is realized without violating thruster capabilities.

Equation (7) describes the linear transformation between the magnitudes of the three jet thrusts, $\mathbf{J} = [J_A, J_B, J_C]^T$, and the control variables $\mathrm{t}_c = [F_x, F_y, M_z]^T$. In order to realize the control algorithm described above, we calculate $\mathbf{J}$, using (7a), according to:

$$\mathbf{J} = \mathbf{B}^{-1}(\varphi_A, \varphi_B, \varphi_C)\mathrm{t}_c \tag{17}$$

It is important for the successful implementation of the control algorithm to keep $\mathbf{J}$, as low as possible. Hence, we examine matrix $\mathbf{B}$. Our goal is to find the appropriate configuration of matrix $\mathbf{B}$ in order to maintain the vector $\mathbf{J}$, with the magnitudes of the thrusts, as low as possible.

In order to keep $\mathbf{J}$ low, $\mathbf{B}^{-1}$ must be minimum, or equivalently, $Det(\mathbf{B})$ must be maximized. In other words, $\mathbf{B}$ should be kept away from singular configurations. Thus, the analysis of matrix $\mathbf{B}$ is based on its determinant. Although other methods to shape $\mathbf{B}$ exist, we choose this determinant-centered method because it results in a computationally effective solution, which is very important in real time applications.

$Det(\mathbf{B})$ depends on the geometry of the floating platform and the rotation angles of the pump jets. It can be computed from the following equation:

$$\begin{aligned}Det(\mathbf{B}) = {} & \cos(\varphi_A)[2Q\sin(\varphi_B)\sin(\varphi_C) - \\ & W\sin(\varphi_C - \varphi_B)] - Q\sin(\varphi_A)\sin(\varphi_C + \varphi_B)\end{aligned} \tag{18}$$

where Q and W depend exclusively on platform geometry, and are equal to:

$$\begin{aligned}Q &= d_{DC} \\ W &= d_{AG} + d_{DG}\end{aligned} \tag{19}$$

The first step of our analysis is to find, using (18), the combinations of φ_A, φ_B, and φ_C that make $Det(\mathbf{B})$ equal to zero, and consequently infinite required jet thrusts values. From (18) we obtain that:

$$\begin{aligned}& Det(\mathbf{B}) = 0 \Rightarrow \\ & \varphi_A = A\tan\left(\frac{2B\sin(\varphi_B)\sin(\varphi_C) - A\sin(\varphi_C - \varphi_B)}{Q\sin(\varphi_C + \varphi_B)}\right)\end{aligned} \tag{20}$$

Figure 4 shows these combinations of the jet angles, where $0 < \varphi_B, \varphi_C < \pi/2$. Avoiding these angle sets we ensure that the control algorithm does not requires infinite jet thrusts values. Similar surfaces can be obtained for the entire jet angles range ($0 - 2\pi$).

The extensive search of $Det(\mathbf{B})$ results in the following interesting conclusion. $Det(\mathbf{B})$ is zero when:

(a) $\varphi_B = 0 \,\&\, \varphi_C = k\pi$, where $k = 1, 2$.

(b) $\varphi_B = k\pi \,\&\, \varphi_C = 0$, where $k = 1, 2$.

(c) $\varphi_B = \varphi_C = k\pi$, where $k = 0,1,2$.

(d) $\varphi_B = \pi \,\&\, \varphi_C = 2\pi$ or $\varphi_B = 2\pi \,\&\, \varphi_C = \pi$.

(e) $(\varphi_A = l\pi/2) \,\&\, (\varphi_B + \varphi_C = k\pi)$, $l = 1,3$ & $k = 1,2,3\ldots$.

(f) $\varphi_i = \varphi_j \,\&\, \varphi_q = \varphi_i - \pi$ where $i, j, q = A, B, C$.

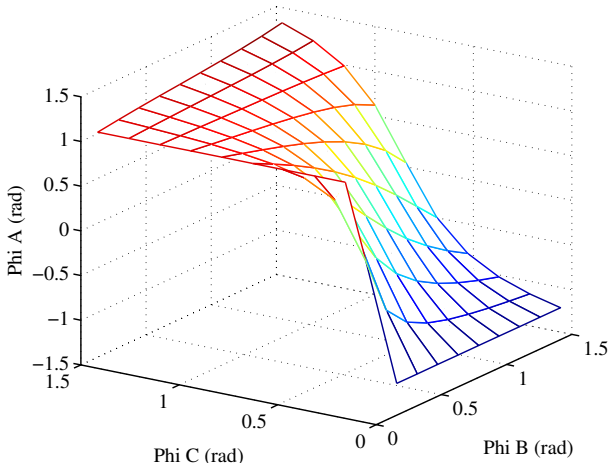

Figure 4. Sets of φ_A, φ_B, and φ_C that make $Det(\mathbf{B})$ equal to zero.

The next step of our analysis is to find the appropriate jet angles sets resulting in maximum $Det(\mathbf{B})$ and guarantee the minimum required jet thrusts values. We consider as acceptable all jet angles sets, which result in a $Det(\mathbf{B})$ that satisfies the following relation:

$$Det(\mathbf{B}(\varphi_A, \varphi_B, \varphi_C)_{ac}) \geq k \max[Det(\mathbf{B}(\varphi_A, \varphi_B, \varphi_C))] \quad (21)$$

where k is a factor high enough to ensure feasible and cost effective jet thrusts values.

Employing an extensive search, we obtain the result shown in Figs. 5 and Fig. 6.

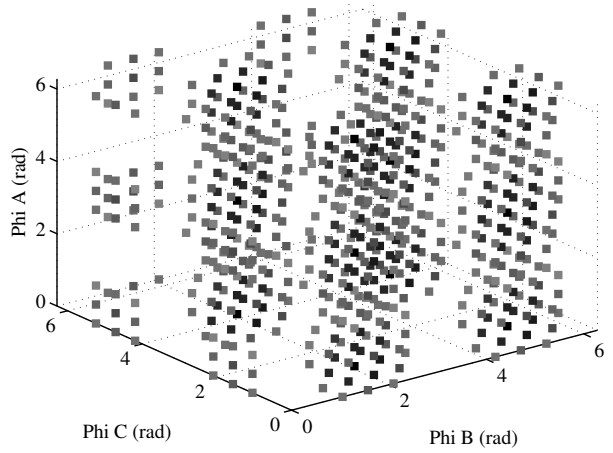

Figure 5. Sets of φ_A, φ_B, and φ_C that make $Det(\mathbf{B})$ higher that 50% of the maximum value ($0 < \varphi_A, \varphi_B, \varphi_C < 2\pi$).

In Fig. 5 all three jet angles are between 0 and 2π (rad). The points shown are representing the resulting angle triplets by setting $k = 0.5$. Since the results shown in Fig. 5 are repeated with a period of π, and for a more clear view, in Fig. 6 all three jet angles are between 0 and π (rad).

Again the points shown are representing the resulting angle triplets by setting $k = 0.5$. In both figures a darker gray color represents a higher value for $Det(\mathbf{B})$. Choosing jet angles triplets from the above shown areas we ensure that the jet thrust values required for the realization of the control algorithm are feasible and cost effective. This is also demonstrated in the next chapter where some simulation runs are described.

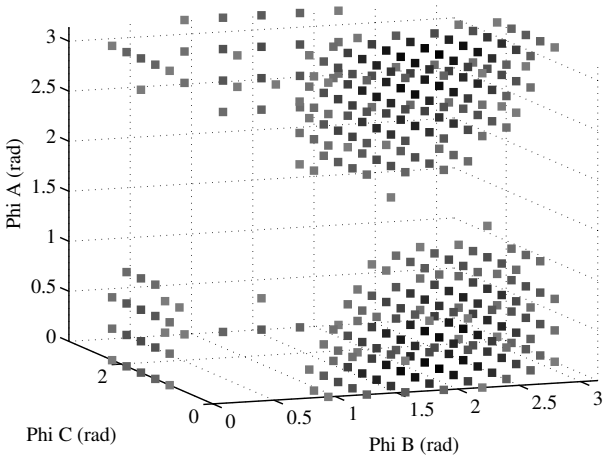

Figure 6. Sets of φ_A, φ_B, and φ_C that make $Det(\mathbf{B})$ higher that 50% of the maximum value ($0 < \varphi_A, \varphi_B, \varphi_C < \pi$).

V. Simulations

In this section we present simulation results to demonstrate the performance of the controlled dynamical system. Some characteristic parameters used are given: geometric data $L_{AB} = 45$, $L_{BC} = 35$, $m = 425 \times 10^3$, $R_{uc} = 2.2$, $H_{uc} = 6.5$, $R_{lc} = 3.5$, $H_{lc} = 3$, all in SI units and the hydrodynamic coefficients are $C_D = 0.8$, $C_A = 0.6$. The gains of the controller were chosen as $k_{dx} = k_{dy} = 0.4$, $k_{d\psi} = 0.2$, $k_{px} = k_{py} = k_{p\psi} = 0.1$, and $k_{ix} = k_{iy} = k_{i\psi} = 0.0$ i.e., no integral action is implemented initially.

The control objective is to drive the platform from some initial configuration to point zero for the position, orientation, and velocity variables. The initial errors are set as $\|x_e\| = 1$, $\|y_e\| = 1$, in m, $\|\psi_e\| = 5$ deg, $\|u_e\| = 0.3$, $\|\upsilon_e\| = 0.2$, in m/s, and, $\|r_e\| = 0.01$ in rad/s. In Fig. 7, the resulting trajectory of the CM of the platform in the inertial 2D space is displayed.

Fig. 8 (a, b, c, d, e, and f) shows the thrusts of the jets and the corresponding angles chosen, according the search results shown in Fig. 6, required to realize the closed loop control forces and moments computed in Section III.

The linear and angular velocities which converge after 40 s, are depicted in Fig. 9 (a, c, and e,) while in Fig. 9 (b, d, and f) we observe the smooth convergence of the position and orientation variables to the desired values after about 40 s as well.

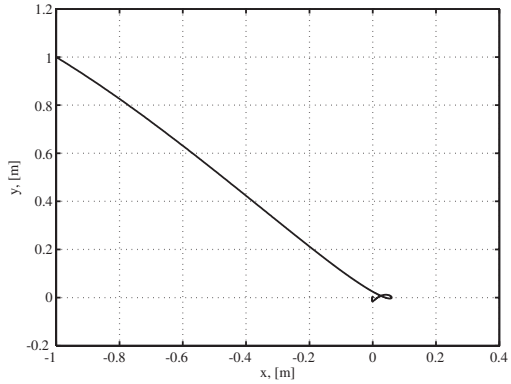

Figure 7. The 2D path of the CM of the platform.

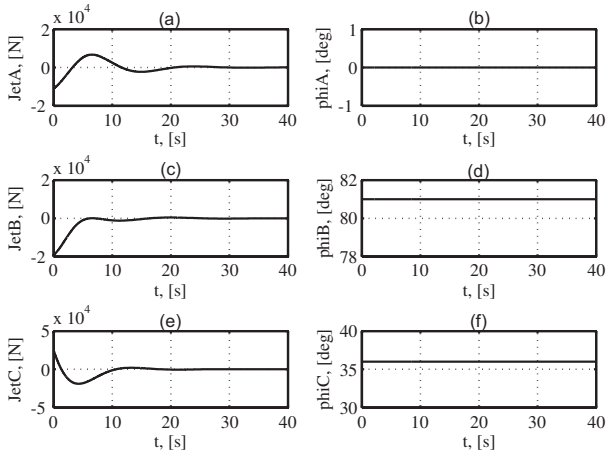

Figure 8. (a), (c), (e) Jet thrusts, and (b), (d), (f) Jet angles.

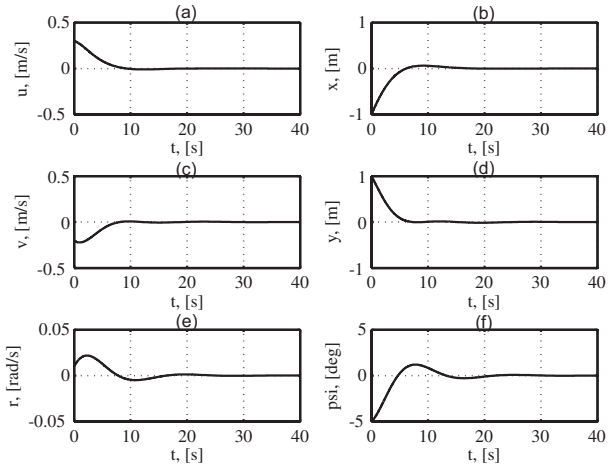

Figure 9. (a), (c), (e) Linear and angular velocities, and (b), (d), (f) Position and orientation variables.

In order to improve the performance of the controller so as to counterbalance environmental disturbances e.g., sea current, we activate next the integral part of the controller setting $k_{ix} = k_{iy} = k_{i\psi} = 0.01$. Also, we impose a sea current with velocity magnitude $v = \sqrt{2}$ m/s. In Fig. 10, the dynamic positioning performance of the added integral action of the controller is illustrated against the sea current disturbances, with the direction indicated on the figure.

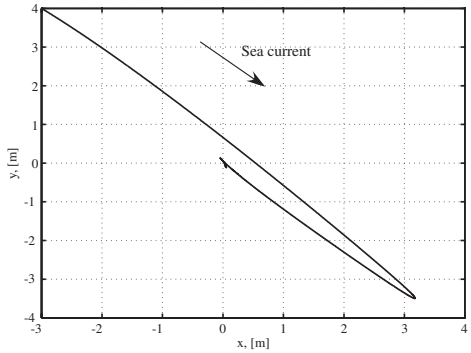

Figure 10. Dynamic positioning with integral action and sea disturbances.

VI. Conclusion

This paper reports initial work on the dynamic modeling and dynamic positioning of a floating triangular platform. The required, closed-loop force and moment is provided by three rotating pump jets, located at the bottom of three partly submerged cylinders located at the corners of the platform. The system is overactuated, i.e., it has more control inputs than degrees of freedom (DOF). Hence, we designed an appropriate and novel control allocation scheme in order for the control objective to be realized without violating thruster capabilities. The scheme is based on the maximization of the determinant of the transformation matrix relating the control forces to the jet thrust. This methodology provides a fast, reliable, and computationally inexpensive algorithm compared to the complex, on-line, iterative ones. Simulation results were presented to demonstrate the performance of the controller and allocation scheme.

References

[1] J. F. Wilson, "Dynamics of Offshore Structures," New Jersey, John Wiley and Sons, 2003.

[2] F. E. Hawary (Ed.), "The Ocean Engineering Handbook," Boca Raton, Florida, CRC Press, 2001.

[3] T. I. Fossen, and T. A. Johansen, "A Survey of Control Allocation Methods for Ships and Underwater Vehicles," in *Proc. Mediterranean Control Conference 2006,* (MED 2006).

[4] M. Bodson, "Evaluation of Optimization Methods for Control Allocation," *Journal of Guidance, Control and Dynamics*, vol. 25, pp. 703–711, 2002.

[5] W. C. Webster and J. Sousa, "Optimum Allocation for Multiple Thrusters," *Proc. of the Int. Society of Offshore and Polar Engineers Conference (ISOPE'99)*, Brest, France, 1999.

[6] T. A. Johansen, T. I. Fossen, and S. P. Berge, "Constraint Nonlinear Control Allocation with Singularity Avoidance using Sequential Quadratic Programming," *IEEE Transactions on Control Systems Technology*, vol. TCST-12, pp. 211–216, 2004.

[7] S. P. Berge and T. I. Fossen, "Robust control allocation of overactuated ships: Experiments with a model ship," *Proc. 4th IFAC Conf. Manoeuvring and Control of Marine Craft*, Brijuni, Croatia, 1997, pp. 166–171.

[8] O. J. Sørdalen, "Optimal Thrust Allocation for Marine Vessels," *Control Engineering Practice*, vol. 5, no. 9, pp. 1223–1231, 1997.

[9] K. M. Lynch, "Controllability of a Planar Body with Unilateral Thrusters," *IEEE Transactions on Automatic Control*, vol. 44, pp. 1206–1211, 1999.

[10] http://www.nestor.noa.gr

[11] S. F. Hoerner, "Fluid-Dynamic Drag," Hoerner Publications, 1965.